

Optimal packing of CO at high coverage on Pt(100) and Pt(111) surfaces

Vaidish Sumaria,[†] Luan Nguyen,[‡] Franklin Feng Tao,[‡] and Philippe Sautet^{*,†,¶}

[†]Department of Chemical and Biomolecular Engineering, University of California, Los Angeles, CA 90094, USA

[‡]Department of Chemical and Petroleum Engineering, University of Kansas, Lawrence, Kansas

[¶]Department of Chemistry and Biochemistry, University of California, Los Angeles, CA 90094, USA

E-mail: sautet@ucla.edu

Abstract

High coverage structures for CO on Pt(111) and Pt(100) surfaces are studied by density functional theory modeling and compared to high pressure scanning tunneling microscopy experiments. Semilocal exchange correlation functionals are known to provide incorrect adsorption site and overestimated adsorption energy for CO on Pt. We develop a simple first-principles correction for the adsorption energy of CO on Pt(111) and Pt(100) using the bond length of adsorbed CO as a descriptor. The energy correction which increases in the order top < bridge < hollow site is used to derive the surface stability diagram for CO adsorbed on 111 and 100 facets of Pt showing the thermodynamically stable CO configurations on the surface as a function of temperature and pressure. High coverage ($\theta > 0.5$) configurations of CO on Pt(111) lead to the formation of superimposed hexagonal/quasi-hexagonal lattice of CO on hexagonal Pt(111) layer from a systematic exploration of such structures. Non-hexagonal structures seen

in vacuum and low temperature conditions - $(\sqrt{3} \times 3)\text{rect-4CO}$ and $c(\sqrt{3} \times 7)\text{rect-5CO}$ are however only $5\text{meV}/\text{\AA}^2$ less stable than the hexagonal lattice at similar coverage. For Pt(100) at $\theta \geq 0.75$, the CO molecules adopt a one dimensional coincidence lattice and we observe the formation of $(n \times 2)$ unit cells ($n=4,6,8$) with $(2n-2)$ CO molecules in each cell on top/quasi-top and bridge/quasi-bridge positions creating a skewed hexagonal lattice to reduce CO-CO repulsion with increasing coverage. The computational results agree with the available experimental observations for Pt(111) and Pt(100). The integrated theoretical simulation and experimental observation provide structural data for the study of catalytic reactivity on Pt surfaces in reactions involving high CO pressures and suggest an approach for understanding the structure of CO molecules on other metal catalyst surfaces during the catalytic reactions involving high pressure of CO.

1 Introduction

Adsorption of carbon monoxide on transition metals is frequently regarded as a benchmark system owing to its importance in CO oxidation¹⁻⁴, water-gas shift reaction⁵⁻⁸ and Fischer Tropsch synthesis⁹⁻¹² and hence has been a subject of many studies, both experimental and theoretical. The determination of the CO adsorption site, coverage and assembly structure on the different transition metal surfaces is a key information for these reactions. It is especially important to understand the structure and coverage of CO at ambient pressure relevant to catalytic conditions. Moreover, the simplicity and known adsorption properties of CO, make it the perfect candidate as a probe molecule in surface science. As a result, adsorption of CO on platinum surfaces (Pt(100) and Pt(111)) is considered as a model system in the field and has been studied using wide range of experimental techniques, some of them enabling to access near ambient to high pressure conditions, including low energy electron diffraction (LEED), X-ray photoemission spectroscopy (XPS), scanning tunnelling microscopy (STM), temperature programmed desorption (TPD), calorimetry, work function measurements, Ex-

tended X-ray absorption fine structure (EXAFS) etc.¹³⁻³⁴. CO adsorption on Pt(111) has been studied both in UHV conditions at low temperature and at atmospheric pressure and room temperature. Interestingly, different structures are seen. In UHV at low temperature, CO initially forms a $(\sqrt{3} \times \sqrt{3})R30^\circ$ -1CO structure at 1/3 ML coverage, occupying the top site, followed by a well ordered $c(4 \times 2)$ -2CO (or equivalently $(\sqrt{3} \times 2)$ rect-2CO) structure at $\theta=0.5$ ML with equal population of top and bridge sites.^{17,18,35,36} The CO arrangement is not hexagonal in this structure. At higher coverage, a set of compressed, but still non-hexagonal, structures is found ($c(\sqrt{3} \times 5)$ rect-3CO, $\theta=0.6$ ML; $(\sqrt{3} \times 3)$ rect-4CO, $\theta=0.67$ ML; $c(\sqrt{3} \times 7)$ rect-5CO, $\theta=0.71$ ML)³⁷. In contrast, at room temperature and atmospheric pressure, STM images show the formation of a hexagonal CO lattice superpositioned on Pt(111) to construct the so called Moiré pattern structures, for example the $(\sqrt{19} \times \sqrt{19})R23.4^\circ$ -13CO commensurate structure at $\theta=0.68$ ML.³⁸ The presence of this different set of CO structures for different conditions is puzzling and the stable or metastable nature of these structures is unclear until now. On the other hand, the situation for CO adsorption at low coverage on Pt(100) is somewhat more confused. Bradshaw et al. showed using vibrational spectroscopy that at 90 K CO occupies the bridge site until 0.5 ML ($c(2 \times 2)$ structure), while at room temperature an equal mixture of bridge and top site is seen.³² Hence the bridge site should correspond to a slightly lower internal energy. At high coverage, adsorbed CO on Pt(100) is reported using STM images to adopt a $c(5\sqrt{2} \times \sqrt{2})R45^\circ$ -3CO unit cell ($\theta = 0.6$ ML) with 2:1 bridge to top site ratio,³¹ followed by a $(3\sqrt{2} \times \sqrt{2})R45^\circ$ -4CO ($\theta = 0.67$ ML) unit cell with a 1:1 bridge to top site ratio and a $c(4 \times 2)$ -3CO unit cell ($\theta = 0.75$ ML) with 2:1 bridge to top site adsorption ratio, using LEED.³² In parallel, synergistic efforts have been applied on the computational aspects of studying the Pt/CO system.³⁹⁻⁴³ A recent work by Gunasooriya et al. used the vdW-DF non-local functional to model ordered CO structures on Pt(111) at the high coverage limit.³⁹

Understanding surface phenomena in heterogeneous catalysis theoretically has been vastly improved owing to the advancement in density functional theory with the semilo-

cal (GGA) and hybrid exchange correlation (XC) functionals. Despite these successes, a few cases of performing these electronic structure calculations are known to be problematic in determining the correct adsorption site. This challenge is famously known for the Pt(111)/CO system and is coined as “The Pt(111)/CO Puzzle.”^{41,44–47}. The widely used semilocal XC functionals - PW91, PBE and RPBE predict chemisorption energies for CO on Pt significantly higher than experimental determination by single crystal calorimetry by approximately 0.37, 0.37 and 0.17 eV respectively.^{48,49}. More importantly, all these functionals favour the more coordinated bridge and hollow sites over the top site for Pt(111). On the other hand, more accurate hybrid functionals (PBE0⁵⁰, B3LYP⁵¹) have been able to predict the correct adsorption site, but provide a CO adsorption energy which is even more overestimated than semilocal functionals, in relation with an overestimated Pt d-band width. Blyholder model^{52,53}, describes CO chemisorption on metal surfaces from CO molecular orbitals. This commonly used model suggests interactions of the two CO frontier orbitals, the 5σ highest occupied molecular orbital (HOMO) and the $2\pi^*$ lowest unoccupied molecular orbital (LUMO), with the metal states. The bonding 5σ orbital (HOMO) donates electron density to the substrate (known as σ -donation) and the anti-bonding $2\pi^*$ orbital (LUMO) receives electron density from the the substrate (known as $2\pi^*$ -backbonding). The extent of backbonding increases with the metallic coordination of the adsorption site (hence is more important for hollow-site) where as the highly directional 5σ metal interaction is stronger for the low coordination site, i.e. top site.^{54–56} Semilocal XC functionals such as PBE tend to underestimate the HOMO-LUMO gap for CO^{41,43,57} and place the unfilled CO $2\pi^*$ orbital too low in energy which makes it too close in energy to the metal d band, resulting in an unrealistic strengthening of the $2\pi^* - d$ band bonding interactions (backbonding) which favors multiply bonded sites.

In order to obtain a better agreement with experiments, several studies have developed energy correction schemes to shift the CO LUMO to higher energies, which results in reducing the backbonding and favouring the experimentally observed top site for adsorption. The first

method was developed by Kresse et al. where by using potentials with different core radii, they discovered that there exists a linear relationship linking the difference between top and hollow site adsorption energies for CO on Pt(111) and the gas-phase energy of the CO $2\pi^*$ orbital.⁴¹ They developed a GGA+U inspired method to tune the CO $2\pi^*$ orbital energy and re-institute the correct top-site for CO adsorption on Pt(111). Following this work, another method developed by Mason et al. argued the use of GGA+U, since the U parameter is not known *a priori*.⁵⁵ They showed that the CO adsorption energy is not only dependent on the LUMO level of the free CO molecules but can also be equivalently linearly related to the CO singlet-triplet excitation energy (ΔE_{S-T}). By extrapolating these linear relationships to the Configuration Interaction (CI) calculated value of ΔE_{S-T} , a correction to the GGA energy for a respective adsorption site (top, bridge or hollow) was developed. This method was also shown to be universally working for a variety of metal surfaces.⁵⁵ Finally it was shown that the suggested correction for the adsorption energy also scales with the CO stretching frequency (which is a function of the adsorption site), which can yield a simpler correction scheme. This idea was elaborated later by Abild-Pedersen et. al., who suggested that the adsorption energy correction (Δ) for RPBE XC functional can be simply expressed as $\Delta = 1.8 - 0.0008 \times \nu_{CO}$, where ν_{CO} is the internal stretch vibration frequency of CO in cm^{-1} .⁴² Gajdoš et. al showed that a linear correlation exists between the CO stretching frequency and C-O bond length which is independent of the coordination of the CO molecule.⁴³, which suggests that a relationship could also exist between the adsorption energy correction and the C-O bond length.

In this work, we first derive this correction scheme for CO adsorption energetics based on the adsorbed C-O bond length. Similarly to Mason et. al., we consider different pseudopotentials for C and O and re-establish a scaling relation between the adsorption energies at various sites and the CO gas singlet-triplet excitation energy which is then extrapolated to the accurate CI value of ΔE_{S-T} to find the correction, based on the first principles, needed to be applied with respect to the GGA energy.⁵⁵ We show in addition that this energy

correction simply scales with the CO bond length, hence enabling a generalized correction applicable for low symmetry CO overlayer, where molecules are not in the high symmetry sites and hence have different CO bond lengths. A generalized correction is developed for the 111 and 100 facets of platinum. Finally using first principle thermodynamic analysis and the developed energy corrections, we construct the surface stability diagram that depicts the stable configurations of CO on the Pt(111) and Pt(100) surfaces as a function of temperature and CO pressure. We first compare our results to experimental studies in the literature. We also performed HP-STM experiments on Pt(100) terraces under a high pressure of CO. The combination between theory and experiments uncovers two high coverage CO structures on Pt(100), that to our knowledge have not been presented before in the literature. They consist of $(n \times 2)$ type unit cells with $(2n-2)$ CO atoms arranged in a unique pattern with CO on (quasi) top and (quasi) bridge sites to reduce adsorbate-adsorbate repulsion.

2 Methods

2.1 Computational Details

Calculations were performed using the Vienna Ab-initio Simulation Package using the general gradient approximation (GGA) Perdew-Burke-Erzenhof (PBE) functional. Two set of calculations were performed: (i) Developing the correction scheme for CO adsorption on Pt surfaces, (ii) Using the developed correction scheme to compute the landscape of the adsorbed CO on Pt surfaces at various pressure and temperature conditions. The calculations for CO adsorption correction scheme are modeled using 1/4 and 1 mono-layer coverage of adsorbed CO on a six Pt layer slab, separated by 12 Å vacuum from its periodic image in the z direction. The two bottom layers of the unit cell were kept fixed, and the top four layers with the adsorbates were allowed to relax with a force criterion of <0.01 eV/Å. A fermi smearing width of 0.2 eV was applied using the Methfessel-Paxton method (order 2). A 3x3 surface supercell was considered for Pt(111) and Pt(100) and their Brillouin zones

were sampled using a 7x7x1 k-point mesh. A 0.25 ML and 1 ML coverage was modeled on a 2x2 and 1x1 surface for both Pt(111) and Pt(100) and the k-points were scaled suitably.

The calculation settings used to develop the surface stability diagram are the same as described above. The k-points are suitably scaled for the various unit cells used. We consider the adsorption of CO molecule on various sites with different coverages. The adsorption energy of CO is referenced to gas phase CO and further details of the thermodynamic analysis have been discussed in the supporting information (SI).

The corrections have been obtained using the scheme developed by Mason et al.⁵⁵ This involves the following steps: (i) Using various pseudopotentials for C and O listed in Table S1 for $\theta = 0.25$ ML and Table S2 for $\theta = 1.00$ ML) we find the scaling relations between the CO adsorption energy on top, fcc and hcp (or hollow) site on Pt(111) (and Pt(100)) and the CO singlet-triplet excitation energy, ΔE_{S-T} (SI, Fig. S1 for $\theta = 0.25$ ML, Fig. S2 for $\theta = 1.00$ ML) (ii) These scaling relations are then extrapolated to find the adsorption energy at $\Delta E_{S-T} = 6.095$ eV (excitation energy value reproduced using Coupled-cluster and CI calculations which are comparable with the experimental values.)⁵⁸ (iii) The correction is defined as the difference between the extrapolated value of the adsorption energy and the energy obtained using the normal PAW settings for C and O (Details of these results have been included in the SI section S1.1).

To create the surface stability diagram, we systematically select structures manually inspired by an extensive literature review of the available experimental data including hypothetical structures, or proposed variants. Using a number of surface science studies including LEED, STM, EELS, RAIRS, XPS and TPD results we generate a sequence of ordered structures with increasing CO coverage. The symmetry of configurations at low coverage also helps sample various structures manually. For Pt(111) we use a number of different unit cells including p(2x2), p(3x3), p(4x4), p(5x5), $(\sqrt{3} \times \sqrt{3})R30^\circ$, $(\sqrt{7} \times \sqrt{7})R19.1^\circ$, $(2\sqrt{3} \times 2\sqrt{3})R30^\circ$, $(\sqrt{13} \times \sqrt{13})R14^\circ$, $(\sqrt{19} \times \sqrt{19})R23.4^\circ$, $(\sqrt{21} \times \sqrt{21})R10.8^\circ$, $(3\sqrt{3} \times 3\sqrt{3})R30^\circ$, c(4x2), $(\sqrt{3} \times 3)\text{rect}$, $c(\sqrt{3} \times 5)\text{rect}$, $c(\sqrt{3} \times 7)\text{rect}$ with CO adsorbed on multiple of symmetric (top,

bridge, fcc and hcp) and quasi-symmetric sites. Since at high coverage, STM images show formation of rotated hexagonal CO layers on the Pt(111) surface, we put a special attention to methodically generate a family of such “Moiré pattern” adsorption structures.³⁸. For Pt(100), at low coverages ($\theta \leq 0.67$), we utilize known experimental results to explore adsorption of CO on various unit cells including $c(2 \times 2)$, $c(3 \times 3)$, $c(2\sqrt{2} \times \sqrt{2})R45^\circ$, $c(3\sqrt{2} \times \sqrt{2})R45^\circ$, $c(5\sqrt{2} \times \sqrt{2})R45^\circ$. At higher coverage ($\theta \geq 0.75$), we show later that CO arranges on an elongated $c(n \times 2)$ unit cell which helps us explore systematically a number of different coverages on $c(n \times 2)$ unit cell with $n=4,5,6,7,8,9,10$.

The Gibbs free energy for gas-phase CO and for adsorbed CO on the surface is obtained from the DFT energies with ZPE and entropy corrections determined from frequency calculations performed for all the considered structures using the Harmonic Oscillator approximation. By displacing the atoms of adsorbate in each direction by a small positive and negative displacement, we determine six frequencies per CO which includes the typical CO stretch frequency and five low-frequency models associated with the Pt-C stretching, frustrated rotation and translation. Low frequency modes have a large effect on the entropy, hence we use Truhlar approximation by defining a cutoff frequency of 100 cm^{-1} such that all the frequencies below the cut-off are uniformly shifted up to the cut-off value before entropy calculation. The configurational entropy does not affect the results for temperatures below 1000 K, hence has been ignored in this analysis. More details of the vibrational calculations can be found in the SI section S2. All the reported values of adsorption energies have been corrected using the respective calculated zero point energies.

2.2 Experimental Details

2.2.1 Sample Preparation

Sample preparation was performed in a high pressure scanning tunneling microscope (HP-STM) system which consists of a HP-STM chamber and sample preparation chamber

equipped with a sputter ion gun, mass spectrometer and electron beam heater. The Pt(100) single crystal (9mm diameter and 1 mm thickness) was purchased from MaTeck GmbH. Sample cleaning procedure consists of Ar^+ sputtering (4×10^{-4} Pa Ar at 1000 eV and 10 mA of emission current) at room temperature for 15 minutes, annealing at 800K under O_2 atmosphere of 2.7×10^{-6} Pa, and annealing at 1200K in UHV for 5 minutes. This procedure was repeated for 5 to 10 cycles. In the last cycle, an additional reduction step at 800K in 2.7×10^{-6} Pa H_2 was performed. The sample cleanness was checked by STM.

2.2.2 High-Pressure Scanning Tunneling Microscope (HP-STM)

Surface structure of Pt(100) under UHV and CO environment (at different pressures) was studied using a HP-STM system. Details information about this system can be found in the literature.⁵⁹ In short, the sample was placed inside the HP-STM cell (approximately 15mL in volume) with the cell door remained open for surface checking under UHV environment. For in-situ experiment, the HP-STM cell door was closed and CO gas was flown through the cell and over the sample during STM image acquisition. The sample could be heated simultaneously by an IR laser (810 nm) irradiation on the back of the sample. The sample temperature was monitored using a K-type thermocouple spot-welded onto the back of the sample.

3 Results and Discussions

3.1 CO adsorption energy correction scheme

Fig. 1 shows the calculated correction for the CO adsorption energy on Pt(111) and Pt(100) for the top, bridge and hollow site, at a coverage of 0.25 ML. This correction scales with very small error to the bond length of the adsorbed CO (MAE equal or smaller than 4 meV). The difference between the correction developed using the two coverages (0.25 and 1 ML) is small (SI, Fig. S3) and hence we use the relations developed for $\theta = 0.25$ ML for all our

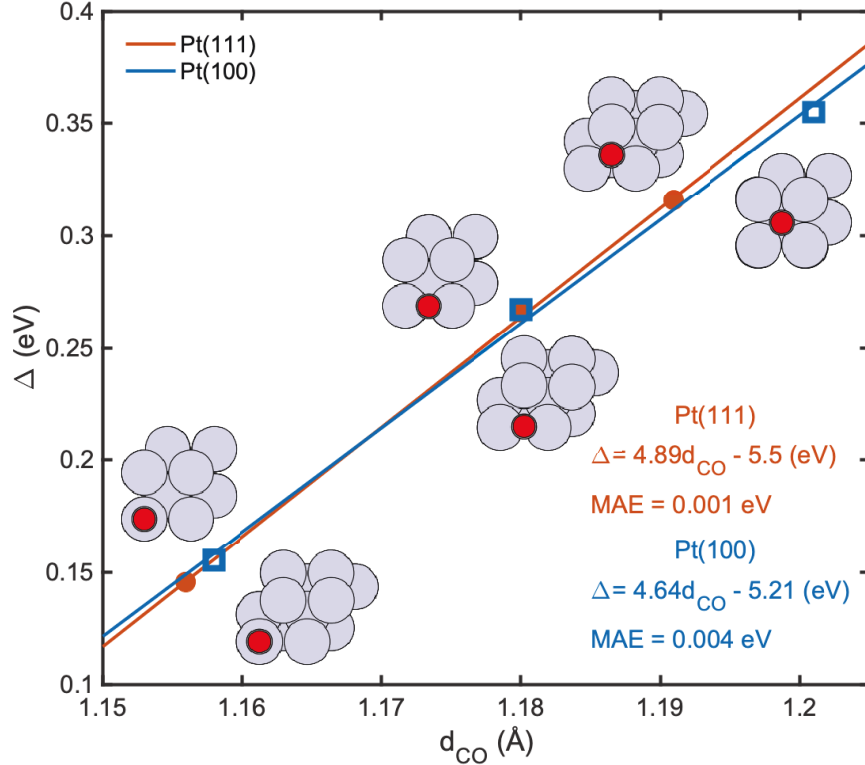


Figure 1: Correction in CO adsorption energy (Δ) plotted against the adsorbed CO bond distance (d_{CO}) for various sites (top, bridge and hollow/hcp) for Pt(100) and Pt(111). The corrections are measured by extrapolating the dependence of the adsorption energy (E_{CO}^{ad}) on the CO singlet-triplet excitation energy (ΔE_{S-T}) for the various sites on (100) and (111) surfaces of Pt to the coupled cluster and CI calculated value for ΔE_{S-T} (refer to SI for more details). CO coverage is 0.25 ML. The red dots (\bullet) and the red line represents the data and the correction as a function of CO bond distance for Pt(111) which is given as $\Delta = 5.13 d_{CO} - 5.83$ where d_{CO} is in Å and Δ in eV. Similarly, the blue squares (\square) represent the correction for the Pt(100) surface and can be expressed as $\Delta = 4.8 d_{CO} - 5.44$. Both the fits have a mean absolute error (MAE) of smaller than 4 meV per CO. The structures (on Pt(111) and Pt(100)) for which the corresponding correction is calculated are shown.

calculations, irrespective of the coverage. Selecting the relation at 1ML coverage does not change the results presented here.

From previous studies, it has been shown that both 5σ -metal d and $2\pi^*$ -metal d interactions are bonding and the donation from 5σ orbital is dominant for CO adsorbed on the top site whereas the back-donation to the $2\pi^*$ is dominant for the hollow sites.^{41,53,60,61} Accordingly the inaccurate DFT-GGA ΔE_{S-T} (or the incorrect placement of $2\pi^*$ orbital) will require the smallest correction for the top site, followed by the bridge and other poly-coordinated

sites (threefold hcp/fcc site for Pt(111) and fourfold hollow site for Pt(100)). This explains the trend we see in the Fig. 1, where the correction required increases with C-O bond distance which is lowest for top site and highest for hcp/hollow site. Another observation is that within the range of C-O bond distance plotted in Fig. 1 (1.15-1.25 Å), the correction calculated at a given value of d_{CO} is fairly constant between Pt(100) and Pt(111) with a max difference of 0.015 eV between the two surfaces. This suggests that we can also develop a general correction scheme that is universal across different facets of Pt which is slightly more approximate but simpler to use. Nevertheless, in the current work, we proceed with using the respective corrections for Pt(111) and Pt(100). Table 1 shows a comparison of the CO adsorption energies obtained experimentally using single crystal adsorption calorimetry (SCAC) and PBE corrected energies. The predicted energies are lowered in absolute value by up to 0.3 eV and brought within 0.15 eV error of the experimental values. On Pt(111) after correction, the adsorption energies of the top, bridge and hollow sites are very similar. On Pt(100), the bridge site remains 0.1 eV more stable than the top site, and the 4-fold hollow site is significantly less stable (by 0.57 eV). We will discuss the site dependence of the energy again below.

Table 1: CO adsorption energies (in eV, including the ZPE correction) on Pt(111) and Pt(100) for top, bridge and hollow adsorption sites as predicted by the PBE exchange correlation functional, after applying the correction to the PBE energies (Corr.) and experimentally obtained value (Expt.).

Pt(111) (0.25 ML)				Pt(100) (0.25 ML)			
	PBE	Corr.	Expt.		PBE	Corr.	Expt.
Top	-1.58	-1.42	-1.27 ± 0.13 ^{42,62}	Top	-1.86	-1.70	-1.57 ± 0.1 ²⁹
Bridge	-1.74	-1.46	-	Bridge	-2.07	-1.80	-
FCC 3-fold Hollow	-1.77	-1.45	-	4-fold Hol- low	-1.60	-1.23	-

3.2 Pt(111) surface stability

In experimental conditions of heterogeneous catalysis, the structure of the catalytic interface is far from that in vacuum.⁶³ Thus to understand the adsorption landscape, we determine

the (T,P) surface stability diagram which covers the surface phases from Ultra High Vacuum and low temperatures to realistic catalytic conditions. Such a thermodynamics based approach in conjunction with ab-initio calculations has been successfully utilized to study Pd hydrogenation catalysts⁶⁴, model RuO₂ structure in O₂ and CO environment⁶⁵, oxygen adsorption on Ag(111)⁶⁶, CO and O₂ induced reconstruction in Pd/Ag(111) surface alloy⁶⁷ etc. This method involves comparing the surface stability for systems with varying number of adsorbates. This is achieved by either comparing the unit surface energy or adsorption energy per unit area for the systems. In this work, we use the adsorption energy per unit area since we are more interested in the CO binding energies rather than energies for the overall formation of these surfaces. Since the exact procedure used is similar to that in previous works, we don't discuss it here again, but include the complete analysis in the SI section S2.

Fig. 2 depicts the thermodynamically most stable state of CO on the Pt(111) surface

Table 2: Stable surface structures observed in Fig. 2 (and shown in table 3). The table outlines the types of unit cells, the CO coverage, the average adsorption energy per CO (including ΔZPE) and the average adsorption Gibbs free energy per CO per unit area of the cell at 300K and 1 atm pressure. Low energy competing metastable structures are also indicated with -a, -b or -c added label

ID	Structure	Coverage	ΔE_{CO}^{avg} (eV)	$\Delta G_{CO}/A$ (eV/Å ²)
I	Bare Pt(111) surface	$\theta = 0.00$	-	
II	$(\sqrt{3} \times \sqrt{3})R30^\circ$ -1CO (T)	$\theta = 0.33$	-1.50	-5.03e-02
II-a	$(\sqrt{21} \times \sqrt{21})R10.8^\circ$ -7CO	$\theta = 0.33$	-1.43	-4.64e-02
III	$c(4 \times 2)$ -2CO (2T-2B)	$\theta = 0.50$	-1.39	-6.67e-02
III-a	(4×2) -2CO (3T-1B)	$\theta = 0.50$	-1.34	-6.32e-02
IV	$(2\sqrt{3} \times 2\sqrt{3})R30.0^\circ$ -7CO (3T-3B-1H)	$\theta = 0.583$	-1.34	-7.16e-02
IV-a	$(2\sqrt{3} \times 2\sqrt{3})R30.0^\circ$ -7CO (4T-2B-1H)	$\theta = 0.583$	-1.31	-7.42e-02
IV-b	$(\sqrt{13} \times \sqrt{13})R14.0^\circ$ -7CO	$\theta = 0.54$	-1.36	-7.00e-02
IV-c	$(\sqrt{7} \times \sqrt{7})R19.1^\circ$ -4CO	$\theta = 0.571$	-1.34	-7.24e-02
V	$(\sqrt{19} \times \sqrt{19})R23.4^\circ$ -13CO (1)	$\theta = 0.684$	-1.23	-7.53e-01
V-a	$(\sqrt{19} \times \sqrt{19})R23.4^\circ$ -13CO (2)	$\theta = 0.684$	-1.21	-1.39e-01
V-b	$(\sqrt{3} \times 3)$ rect-4CO	$\theta = 0.677$	-1.23	-7.40e-02
V-c	$c(\sqrt{3} \times 7)$ rect-5CO	$\theta = 0.677$	-1.23	-7.40e-02
VI	$p(2 \times 2)$ -3CO	$\theta = 0.750$	-1.16	-7.47e-02

(lowest adsorption Gibbs energy per unit area) as a function of operational temperature and pressure as predicted after applying the aforementioned correction in the DFT calculated adsorption energies. In total, 61 potential structures were generated (including the bare Pt(111) surface), spanning a coverage between 0 and 1 ML (SI table S3). We put a special attention to systematically generate, among others, all CO adsorption configurations resulting from the matching between an arbitrary (rotated) supercell of Pt(111) and another (rotated) supercell of an hexagonal CO layer, hence generating a family of “Moiré pattern” adsorption structures. Among these 61 structures, 6 are the most stable one in a region of the (T,P) diagram of Fig. 2 and are also presented in table 2. Some structures are very close in energy to these most stable ones. We also include in table 2 the structures which surface free energy is at most $5 \text{ meV}/\text{\AA}^2$ less stable than the most stable one found in any point of the diagram. Due to inaccuracies in the calculations, it is indeed not possible to exclude that these structures could be found experimentally stable. As expected, with the increase in the chemical potential of CO ($\sim -2.7 \text{ eV}$ at 600K and 10^{-6} Pa , to $\sim 0 \text{ eV}$ at 100K and 10^8 Pa), we see that the coverage of CO on Pt(111) increases. An interesting feature of the stable structures emerging from our results is that CO tends to form a quasi-hexagonal structure on the Pt(111) surface at high coverages. These hexagonal CO patterns either match the Pt hexagonal orientation on the (111) surface or are rotated at an angle to create a so called family of “Moiré patterns”.

At low pressure and high temperature conditions we find that it is thermodynamically not favorable to have CO adsorbed on the surface (bottom right corner of Fig. 2). With increasing pressure and decreasing temperature, CO first arranges on a $(\sqrt{3} \times \sqrt{3}) R30^\circ$ unit cell with CO only on the top site (structure (II) in Table 3). The very small preference in the internal energy for the bridge site (Table 2) is counterbalanced by a larger vibrational entropy at the top site, resulting in a most stable top site. This matches the experimentally observed structure first seen in UHV conditions upon dosing CO at a $1/3 \text{ ML}$ ($\theta = 0.33$) coverage.¹⁷ At 300 K, for $-1.43 < \Delta\mu_{CO}(T, P) < -1.08 \text{ eV}$, the $(\sqrt{21} \times \sqrt{21})R10.8^\circ$ -7CO

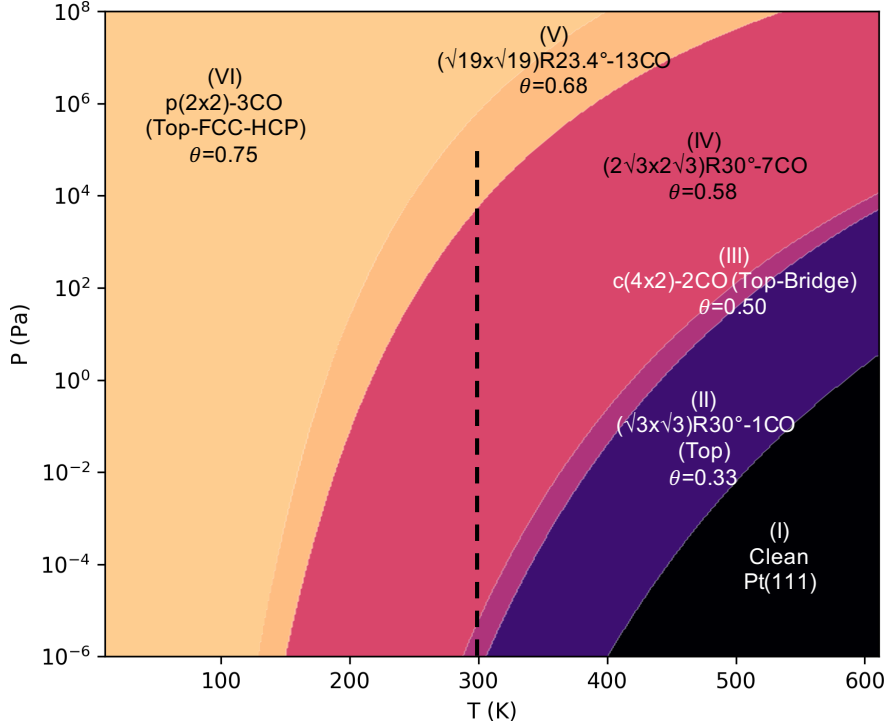


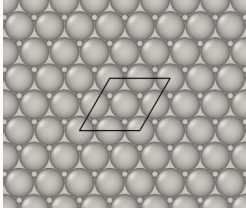
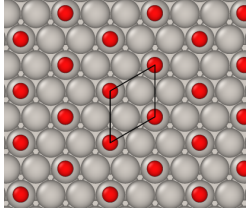
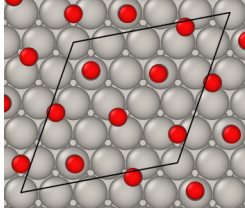
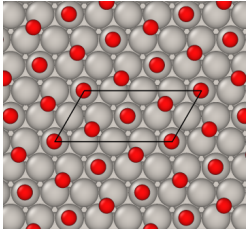
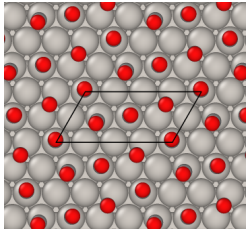
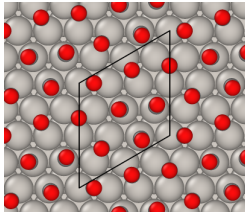
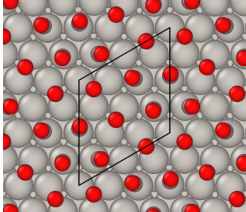
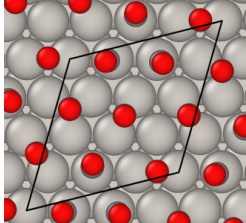
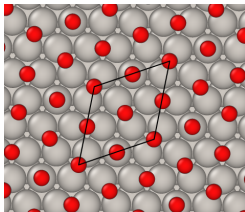
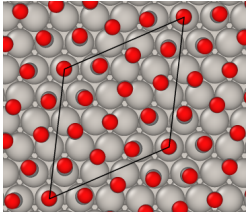
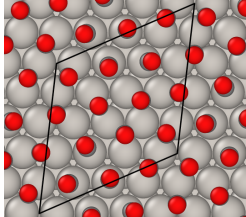
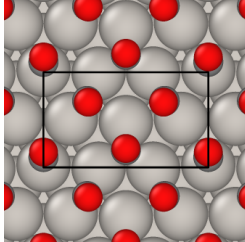
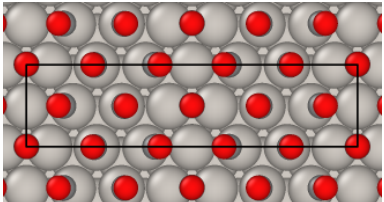
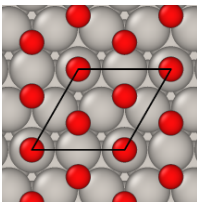
Figure 2: Thermodynamic surface stability diagram depicting the most stable CO coverage as a function of temperature and pressure on Pt(111). The various colors represent the calculated most stable surface terminations as labelled in the figure and shown in table 2. The black dashed line represents the pressure range studied using STM at 300 K by Longwitz et. al. where the superposition of quasi-hexagonal (and hexagonal) lattice of CO on the hexagonal lattice of Pt(111) appears in range of coverage from 0.5 to 0.68 ML.

structure ((II-a) in Table 3) is only 4 meV/Å² less stable than the ($\sqrt{3} \times \sqrt{3}$) $R30^\circ$ structure. On ($\sqrt{21} \times \sqrt{21}$) $R10.8^\circ$ -7CO unit cell, CO arranges on a combination of top and bridge site to form a hexagonal pattern. Further increase in the pressure and decrease in temperature results in half-monolayer coverage with c(4x2)-2CO unit cell that consists of equal population of top and bridge sites (structure (III) in Table 3) which agrees with the experimental studies using LEED, EELS and STM.^{18,68–70} At this same coverage at 300 K, for a small range of chemical potential of CO ($-1.08 < \Delta\mu_{CO}(T, P) < -1.01$ eV), a metastable c(4x2)-2CO structure with 3 CO on top (and quasi top) site and one CO on bridge site (structure (III-a) in Table 3) is found 3.5 meV/Å² higher in energy. The CO layer in this stable mixed top-bridge structure is strongly deviating from an hexagonal arrangement. One CO molecule is surrounded by 6 other CO molecules, but the structure is markedly distorted with neighbors

at a $\sqrt{3}$ separation (4.881 Å) and others at $\sqrt{7}/2$ (3.727 Å). This is the last structure of this type on the diagram of figure 2 and all other structures found stable at higher coverage will all be (quasi) hexagonal.

The next domain corresponds to structure IV and enters the conditions studied by Longwitz et al.³⁸ using STM at room temperature. We will hence follow the dotted black line on Fig. 2. Along this line (at 300 K), in the pressure range 10^{-5} to 6×10^3 Pa, corresponding to $-1.01 \lesssim \Delta\mu_{CO}(T, P) \lesssim -0.47$, we find the $(2\sqrt{3} \times 2\sqrt{3})R30^\circ\text{-7CO}$ structure as most stable (structure (IV) in table 3). On this unit cell CO molecules occupy 3 (quasi) top, 3 bridge and 1 HCP site forming a quasi-hexagonal arrangement. On the same unit cell, another structure with CO occupying 4 (quasi)top, 2 bridge and 1 HCP site (structure IV-a in table 3) is only $0.5 \text{ meV}/\text{Å}^2$ less stable than the former structure, thus quasi-isoenergetic. STM images show in this pressure range a Moiré pattern image corresponding to a superstructure rotated by 30° with respect to the Pt lattice, in good agreement with our theoretical geometry, but with a lattice vector length increasing continuously from 3.2 to 4 times the Pt-Pt distance and CO coverage from 0.56 to 0.65 ML, explained by the incommensurate nature of the imaged structure, instead of constant values of 3.46 Å and 0.58 ML in our case. The CO dense rows are rotated by $10\text{-}15^\circ$ with respect to Pt rows, which agree well with our 11.63° value. Our computed structure can hence be viewed as a (necessarily) commensurate approximate of an otherwise incommensurate phase evolving with pressure. In this chemical potential range ($-1.01 \lesssim \Delta\mu_{CO}(T, P) \lesssim -0.47$), we also see some slightly less stable structures with coverages between 0.5 ML and 0.58 ML. At $\theta = 0.54$, the $(\sqrt{13} \times \sqrt{13})R14^\circ\text{-7CO}$ structure ((IV-b) in Table 3) is at most $9.5 \text{ meV}/\text{Å}^2$ less stable, at $\theta = 0.57$, the $(\sqrt{7} \times \sqrt{7})R19.1^\circ\text{-4CO}$ structure ((IV-c) in Table 3) is at most $2 \text{ meV}/\text{Å}^2$ less stable compared to the predicted structure at 0.58 ML. These low energy metastable structures have not been seen experimentally, to our knowledge. At a pressure above 6×10^3 Pa, the overlayer switches to another higher coverage superposition structure $(\sqrt{19} \times \sqrt{19})R23.4^\circ\text{-13CO}$ ((V) in Table 3), with coverage of $\theta = 0.684$ (13 CO on a 19 surface Pt atoms), which remains stable until 6×10^5 Pa, corresponding to

Table 3: Low energy structures for CO on Pt(111) for various coverages. This includes stable structures found in the surface stability diagram of Fig. 2 (using the same numeric ID) and low energy metastable structures with surface energy at most $5 \text{ meV}/\text{\AA}^2$ less stable (indicated with the added -a and -b labels).

<p>(I) Clean</p> 	<p>(II) $(\sqrt{3} \times \sqrt{3})\text{R}30^\circ\text{-1CO}$ (T)</p> 	<p>(II-a) $(\sqrt{21} \times \sqrt{21})\text{R}10.8^\circ\text{-7CO}$</p> 
<p>(III) $c(4 \times 2)\text{-2CO}$ (2T-2B)</p> 	<p>(III-a) $c(4 \times 2)\text{-2CO}$ (3T-1B)</p> 	<p>(IV) $(2\sqrt{3} \times 2\sqrt{3})\text{R}30.0^\circ\text{-7CO}$ (3T-3B-1H)</p> 
<p>(IV-a) $(2\sqrt{3} \times 2\sqrt{3})\text{R}30.0^\circ\text{-7CO}$ (4T-2B-1H)</p> 	<p>(IV-b) $(\sqrt{13} \times \sqrt{13})\text{R}14.0^\circ\text{-7CO}$</p> 	<p>(IV-c) $(\sqrt{7} \times \sqrt{7})\text{R}19.1^\circ\text{-4CO}$</p> 
<p>(V) $(\sqrt{19} \times \sqrt{19})\text{R}23.4^\circ\text{-13CO}$</p> 	<p>(V-a) $(\sqrt{19} \times \sqrt{19})\text{R}23.4^\circ\text{-13CO}$</p> 	<p>(V-b) $(\sqrt{3} \times 3)\text{rect-4CO}$ (1T-3B)</p> 
<p>(V-c) $c(\sqrt{3} \times 7)\text{rect-5CO}$</p> 	<p>(VI) $p(2 \times 2)\text{-3CO}$</p> 	

the CO chemical potential interval of $-0.47 \lesssim \Delta\mu_{CO}(T, P) \lesssim -0.34$. The coincidence lattice places the CO adsorbate on various adsorption sites ((quasi)top, bridge, fcc, hcp), but 7 of the 13 CO molecules are on the top or quasi-top sites. This commensurate structure is clearly seen in the STM experiment at RT and 9.6×10^4 Pa.³⁸ The simulated STM image (SI fig. S6) of this structure also compares well with the experiment. As shown earlier by Bocquet et al. in the case of low coverage CO, the bright spot on the image corresponds to CO on the top/quasi-top site and the lesser bright spot corresponds to the bridge/quasi-bridge/hollow site.⁴⁰ On the same unit cell, another orientation of CO with 5 of the 13 CO on the top or quasi-top sites ((V-a) in Table 3) is observed to be slightly less stable with an energy difference of only $1.4 \text{ meV}/\text{\AA}^2$. Starting from the previously described incommensurate Moiré pattern rotated by 30° (at $\theta=0.5$), the experimental structure undergoes a rotational phase transition at $\theta \sim 0.6$ - 0.65 ML, with a decrease of the superstructure angle with respect to the Pt lattice from 30° to 23.4° and the stabilization of the lattice vector length at 4.36 times the Pt-Pt distance. This is in very good agreement with the calculated structural parameters for the $(2\sqrt{3} \times 2\sqrt{3})R30^\circ$ -7CO and $(\sqrt{19} \times \sqrt{19})R23.4^\circ$ -13CO coincidence lattices. Hence, for coverage above 0.5 ML, structures calculated to be most stable correspond to the quasi-hexagonal ones seen by the room temperature atmospheric pressure experiments. Let us now compare with the non-hexagonal structures found in UHV and high pressure.

At a coverage of 0.6, three different models have been proposed for a $c(\sqrt{3} \times 5)$ rect-3CO unit cell with bridge:top occupation ratio of 2:1 (proposed by Petrova and Yakovkin⁷¹, shown in SI table S3 ID: 38) and 1:2 (proposed by Persson et al.³⁷ and Avery et al.¹³ having different CO relative positions, shown in SI table S3 ID: 39,40 respectively). Structures 39 and 40 are found to be quasi-isoenergetic and more stable than 38. Gunasooriya et. al using computational thermodynamics shows that the structures with a bridge:top ratio of 1:2 are stable.³⁹ However, our calculations show that the $(\sqrt{19} \times \sqrt{19})R23.4^\circ$ -13CO overlayer is significantly more stable (with an energy difference of $16.8 \text{ meV}/\text{\AA}^2$ at 300K) compared to the $c(\sqrt{3} \times 5)$ -3CO structure, and the later is thus not visible in the surface stability

diagram. Similarly, at a coverage of 0.67, on the basis of LEED and HREELS studies, Avery¹³ suggested the formation of a $(\sqrt{3} \times 3)$ rect-4CO type unit cell with 1:3 bridge:top site occupation (shown in table 3 V-b). On the same unit cell, Biberian and van Hove²⁰ showed a 3:1 bridge:top occupation using LEED and TPD studies (SI, table S3, structure 50). Our results find the Avery structure slightly more stable than that of Biberian and van Hove, in agreement with the calculations by Gunasooriya et. al. On comparing the $(\sqrt{19} \times \sqrt{19})R23.4^\circ$ -13CO with the $(\sqrt{3} \times 3)$ rect-4CO structure, we find the former structure is numerically more stable but only by a small energy difference of 3 meV/Å².³⁹ At a higher coverage of 0.714 ML, Persson et. al showed LEED studies that suggest a $c(\sqrt{3} \times 7)$ rect-5CO (shown in table 3 V-c).³⁷ Comparing this structure with the $(\sqrt{19} \times \sqrt{19})R23.4^\circ$ -13CO structure shows that the latter is only 2.4 meV/Å² (maximum) more stable. Hence, CO on Pt(111) at high coverage can present two types of structures (hexagonal and non hexagonal) with very similar stability. Our calculation find the hexagonal Moiré pattern type structures to be more stable, but non-hexagonal structures (as $(\sqrt{3} \times 3)$ rect-4CO and $c(\sqrt{3} \times 7)$ rect-5CO) come very close in energy, quasi degenerate. This explains the fact that these two types of structures can be found in different experimental conditions.

At low temperatures and very high $\mu_{CO}(T, P) \gtrsim -0.34$ (at 300K), we find a (2x2) structure with 3 CO molecules on a top, an fcc and an hcp hollow site. Such a structure, has been reported in aqueous acidic medium for Pt(111) using STM along with IRAS⁷² and for Pd(111) using computational results as well as RAIRS/HREELS spectra.⁷³ From all the considered coverages of CO, we find that the adsorption saturates at this coverage of 0.75 ML. Comparing this structure with $c(\sqrt{3} \times 7)$ rect-5CO (0.714 ML), in the chemical potential range ($\mu_{CO}(T, P) \gtrsim -0.34$ (at 300K)) where the former is stable, we find that 0.75 ML structure is only 4.8 meV/Å² (maximum) more stable. This once again reinforces the possible presence of quasi degenerate hexagonal and non-hexagonal packing of CO at high coverages on Pt(111).

The effect the developed correction scheme has a marked effect on the stability diagram

of Pt(111). The stability diagram without the the suggested correction has a very different appearance (supporting information fig. S8). Low coverage phases appear before 1/3 ML, and the fcc hollow site is the preferred site over the experimentally observed top site. Without the applied corrections, the $c(4 \times 2)$ 0.5 ML coverage domain does not appear, which also disagrees with the experimental findings. At $\theta = 0.58$, the $(2\sqrt{3} \times 2\sqrt{3})R30^\circ$ -7CO Moiré pattern is predicted but for a much smaller range of temperature and pressure; and the $(\sqrt{19} \times \sqrt{19})R23.4^\circ$ -13CO structure at $\theta = 0.68$ is not seen, at the benefit on a stongly extended domain for the high coverage $p(2 \times 2)$ (0.75 ML), which appears at 300 K for a pressure of CO 8 orders of magnitude lower than when including the correction. Hence application of the correction has a major qualitative effect on the predicted stability diagram and markedly improves the agreement with experimental results. Using the generalized correction, $\Delta = 4.77d_{CO} - 5.37$ eV, valid for both Pt(111) and Pt(100), results in the same stability diagram, showing that a single surface independent correction appears sufficient.

3.3 Pt(100) surface stability

Fig. 3 depicts the most thermodynamically stable state of the CO on Pt(100) surface as a function of temperature and CO pressure, while adsorption energies and geometries are provided in table 4 and 5 respectively. 29 structures have been generated in total (including the bare Pt(100) surface), and 12 appear on the stability diagram (SI table S4). For high temperature and low pressure the clean surface is the most stable (bottom right corner of Fig. 3). Increasing the chemical potential $\Delta\mu_{CO}(T, P)$ (reducing the temperature or increasing the pressure), we find two narrow stable domains corresponding to low coverage adsorption of CO at 0.11 and 0.25 ML. CO is calculated to adsorb slightly more favorably on the bridge site. The first wide domain of stability corresponds to the $c(2 \times 2)$ -1CO structure ($\theta=0.5$ ML) with both CO on bridge sites. The difference in energy between CO on top vs CO on bridge site (structure IV and IV-a in table 4) is again small 2.5 meV/Å². IRAS experiments for low coverage CO adsorption (until 0.5 ML) on Pt(100) at 90 K gives rise to a single

band at 1874 cm^{-1} , assigned to bridge bonded CO, in good agreement with the calculated frequency of 1863 cm^{-1} .³² A band at 2075 cm^{-1} , assigned to top site CO, only appears at higher exposure. Low coverage adsorption at 300 K gives rise to two bands, one at 2067 cm^{-1} , for top site, and another at 1870 cm^{-1} , for bridge-site CO. From these experiments, Martin et al. concluded that the ratio of bridge to linear site occupancy at low coverages is temperature-dependent with a favored $c(2\times 2)$ (or equivalently $(\sqrt{2} \times \sqrt{2})R45^\circ$) 0.5 ML structure with bridge sites at low temperature, and a superposition of bridge site and top sites domains at high temperature.³² This agrees with a slightly more stable energy for bridge site at low coverage. For this 0.5 ML coverage, a $(2\sqrt{2} \times \sqrt{2})$ unit cell can provide a different arrangement of bridge sites which is almost degenerate (IVb in table 5). A $p(2\times 2)$ -2CO unit cell with equal population of top and bridge site (SI table S4 structure 11) is also compared with the symmetric $c(2\times 2)$ -1CO structures, and the former structure is found only $4\text{ meV}/\text{\AA}^2$ less stable.

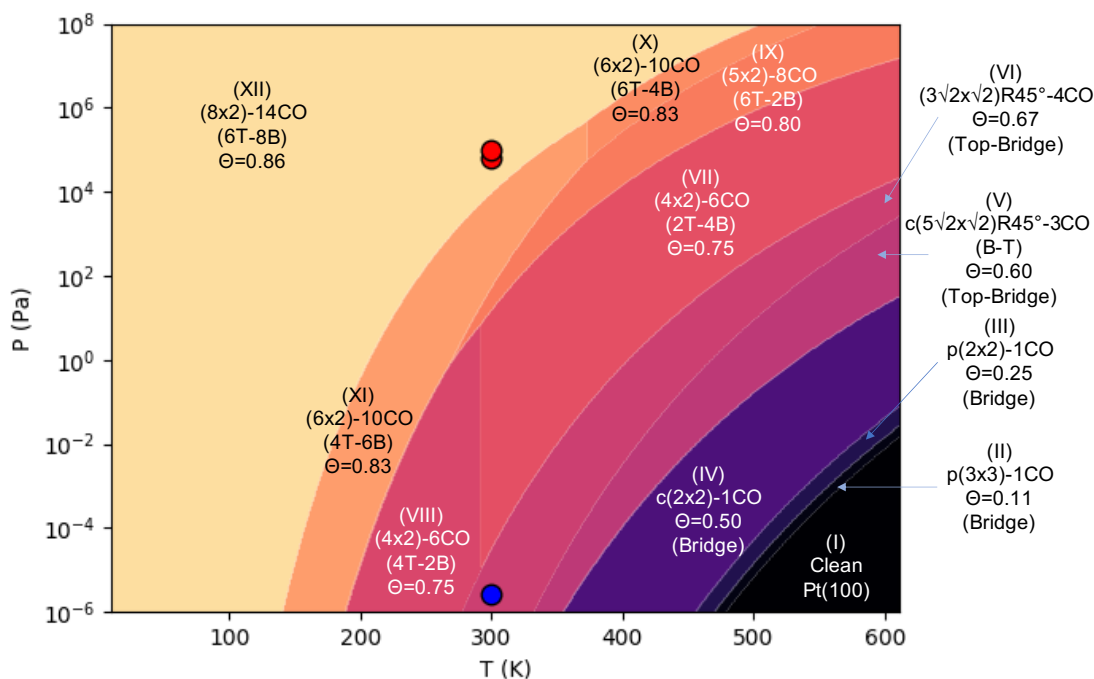


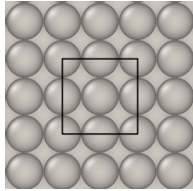
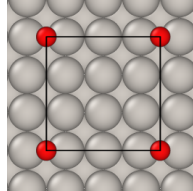
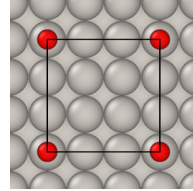
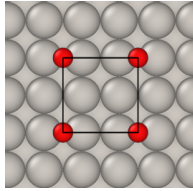
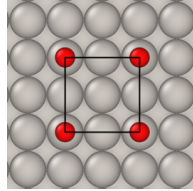
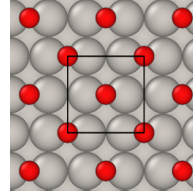
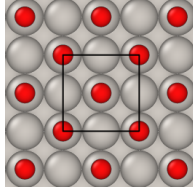
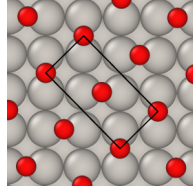
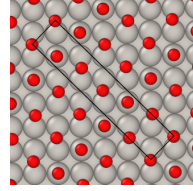
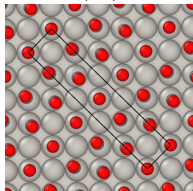
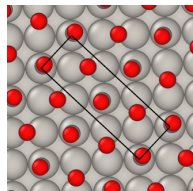
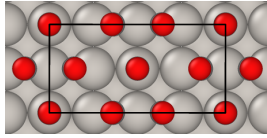
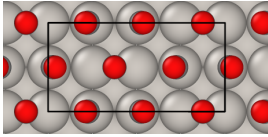
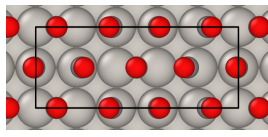
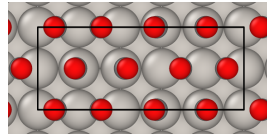
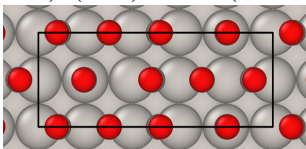
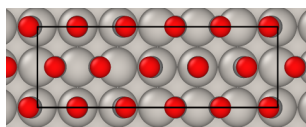
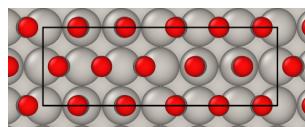
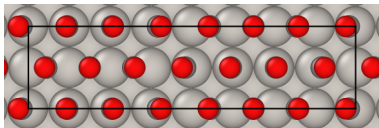
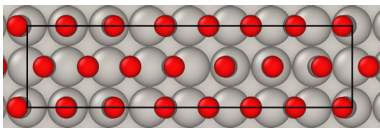
Figure 3: Thermodynamic surface stability diagram depicting the most stable CO coverage as a function of the temperature and pressure on Pt(100). Above $\theta \geq 0.75$, we see formation of the $c(n\times 2)$ unit cells with $(n-2)\text{CO}$ ($n=4,6,8$) which are observed in STM images discussed in the paper. The red and blue dots on the plot represent the different pressures at room temperature where HP-STM images were obtained.

Table 4: Stable surface structures observed in Fig. 3 (and shown in table 5). The table outlines the types of unit cells, the CO coverage, the average adsorption energy per CO (including ΔZPE) and the average adsorption Gibbs free energy per CO per unit area of the cell at 300K and 1 atm pressure. Low energy metastable structures are also (indicated with -a or -b added label).

ID	Unit Cell	Coverage	ΔE_{CO}^{avg} (eV)	$\Delta G_{CO}/A$ (eV/Å ²)
I	Bare Pt(100) surface	$\theta = 0.00$	-	-
II	p(3×3)-1CO (B)	$\theta = 0.11$	-1.82	-0.019
II-a	p(3×3)-1CO (T)	$\theta = 0.11$	-1.71	-0.018
III	p(2×2)-1CO (B)	$\theta = 0.25$	-1.80	-0.042
III-a	p(2×2)-1CO (T)	$\theta = 0.25$	-1.70	-0.039
IV	c(2×2)-1CO (B)	$\theta = 0.50$	-1.76	-0.081
IV-a	c(2×2)-1CO (T)	$\theta = 0.50$	-1.71	-0.078
IV-b	(2√2 × √2)R45°-2CO (B)	$\theta = 0.50$	-1.75	-0.081
V	c(5√2 × √2)R45°-3CO (B-T)	$\theta = 0.60$	-1.68	-0.092
V-a	c(5√2 × √2)R45°-3CO (T)	$\theta = 0.60$	-1.61	-0.086
VI	(3√2 × √2)R45°-4CO	$\theta = 0.67$	-1.64	-0.098
VII	(4×2)-6CO (2T-4B)	$\theta = 0.75$	-1.58	-0.104
VIII	(4×2)-6CO (4T-2B)	$\theta = 0.75$	-1.57	-0.104
IX	(5×2)-8CO (6T-2B)	$\theta = 0.8$	-1.52	-0.106
IX-a	(5×2)-8CO (4T-4B)	$\theta = 0.8$	-1.51	-0.105
IX-b	(5×2)-8CO (2T-6B)	$\theta = 0.8$	-1.50	-0.103
X	(6×2)-10CO (6T-4B)	$\theta = 0.83$	-1.49	-0.106
XI	(6×2)-10CO (4T-6B)	$\theta = 0.83$	-1.48	-0.106
XII	(8×2)-14CO (6T-8B)	$\theta = 0.875$	-1.44	-0.107
XII-a	(8×2)-14CO (8T-6B)	$\theta = 0.875$	-1.44	-0.106

The next stable surface on the diagram (Figure 3) we find is the c(5√2 × √2)R45°-3CO unit cell with $\theta=0.6$ ML. On this unit cell, we compare two different CO adsorption: (i) 4 CO on bridge site and 2 on Top and (ii) all 6 CO on the top site ((V) and (V-a) in Table 5). When compared at 300 K, the former structure is only 6 meV/Å² more stable than the latter corresponding to an overall average adsorption energy difference on 0.07 eV/CO. STM images and LEED analysis confirm the formation of this c(5√2 × √2)R45°-3CO unit cell with a 2:1 bridge to top ratio of CO occupation.^{31,32} On increasing the chemical potential further, CO coverage increases to 0.67 ML on a (3√2 × √2)R45° unit cell with equal ratio of CO on bridge and top sites. This agrees with the experimental analysis from LEED.^{32,74}

Table 5: Low energy structures for CO on Pt(100) for various coverages. This includes stable structures in the surface stability diagram of Fig. 2 (using the same numeric ID) and low energy metastable structures with surface energy at most $5 \text{ meV}/\text{\AA}^2$ less stable (indicated with the added -a and -b labels)

(I) Clean Pt(100) 	(II) p(3x3)-1CO (B) 	(II-a) p(3x3)-1CO (T) 
(III) p(2x2)-1CO (B) 	(III-a) p(2x2)-1CO (T) 	(IV) c(2x2)-1CO (B) 
(IV-a) c(2x2)-1CO (T) 	(IV-b) $(2\sqrt{2} \times \sqrt{2})\text{R}45^\circ\text{-2CO}$ 	(V) $c(5\sqrt{2} \times \sqrt{2})\text{R}45^\circ\text{-3CO}$ (B-T) 
(V-a) $c(5\sqrt{2} \times \sqrt{2})\text{R}45^\circ\text{-3CO}$ (T) 	(VI) $(3\sqrt{2} \times \sqrt{2})\text{R}45^\circ\text{-4CO}$ 	(VII) (4x2)-6CO (2T-4B) 
(VIII) (4x2)-6CO (4T-2B) 	(IX) (5x2)-8CO (6T-2B) 	(IX-a) (5x2)-8CO (4T-4B) 
(IX-b) (5x2)-8CO (2T-6B) 	(X) (6x2)-10CO (6T-4B) 	(XI) (6x2)-10CO (4T-6B) 
(XII) (8x2)-14CO (8T-6B) 	(XII-a) (8x2)-14CO (6T-8B) 	

For $\theta \geq 0.75$, a specific structural pattern was seen for the formation of a dense layer of CO on Pt(100): the registry of a deformed quasi hexagonal CO layer on the Pt(100) surface. We observed the formation of elongated $(n \times 2)$ unit cells with $[(n \times 2) - 2]$ CO adsorbed on a combination of top, quasi-top and bridge sites in Fig. 4. Some structures are centered ($c(n \times 2)$) but for simplicity in the presentation, we will call all of them $(n \times 2)$. At $\theta = 0.75$ a (4×2) -6CO unit cell with 6 CO is observed to be stable. Two different configurations of CO on the surface are observed - (i) 2 CO on top, 4 CO on quasi-bridge site (ii) 4 CO on quasi-top, 2 CO on bridge site (structures VII and VIII shown in table 5). The former is stable at low pressures below 300 K and the later is stable at higher pressures above 300 K. Such an arrangement of CO molecules on the surface results from a compromise between the CO-surface interaction and the repulsive lateral interactions between the CO molecules. It can be seen that any two CO molecules on the short direction of the unit cell are on different sites (bridge or top), which allows for a reduced repulsion of the adsorbates. In addition, this over-layer CO structure was confirmed by in-situ HP-STM result as seen in Fig. 4(a). Gaseous CO was introduced into the HP-STM cell and maintained at 2.7×10^{-6} Pa (2.7×10^{-8} mbar) during image acquisition. At this condition, STM image of Pt(100) shows formation of a domain of (4×2) -6CO over-layer structure, in conditions which are at the border of the calculated region of the phase diagram (red dot in Fig. 3). Red circles in Fig. 4(a) indicate the location of adsorbed CO molecules. The structure present some imperfect order but the assignment is supported by the average CO-CO distance of the CO over-layer (experimental value 0.328 nm, model value 0.338 nm) (Fig. 4(a) and model VII of table 5).

The next stable configuration of adsorbed CO is found on (5×2) -8CO with a coverage of 0.8 ML. At this coverage we find three different configurations of CO on the surface that are identical in energy - CO adsorbed on (i) 6T-2B (ii) 4T-4B (iii) 2T-6B, where T represents top and quasi top site and B represents the bridge and quasi-bridge site of adsorption (structures IX, IX-a, IX-b in Table 5). When compared at 300K, the Gibbs free energy difference between these structures is less than $2 \text{ meV}/\text{\AA}^2$, making them computationally identical. We observe

that this structure is only stable at pressures above 1 Pa and temperatures above RT.

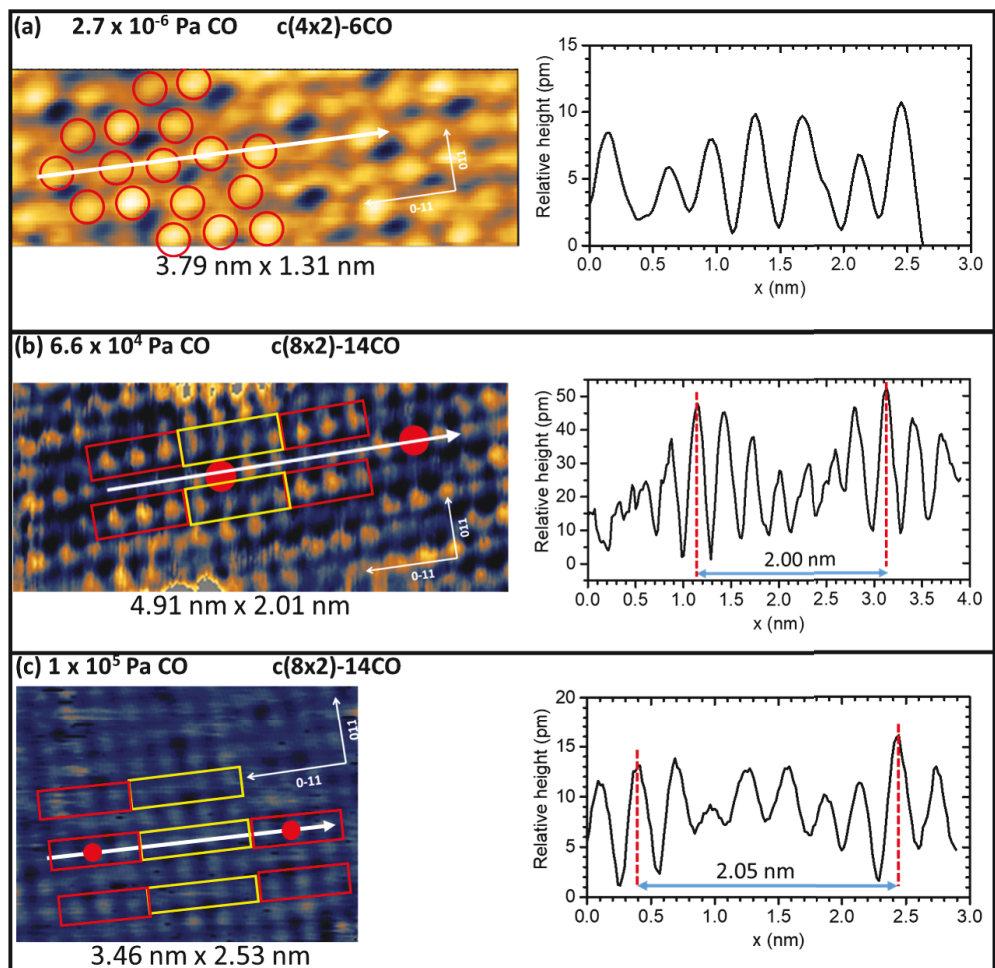


Figure 4: Over-layer structure of CO at different pressure on Pt(100) surface observed by in-situ HP-STM at room temperature. (a) 2.7×10^{-6} Pa CO, which indicates formation of $c(4 \times 2)$ -6CO over-layer corresponding to $\theta = 0.75$. Red circles show location of adsorbed CO molecules. (b) 6.6×10^4 Pa CO, which indicates formation of $c(8 \times 2)$ -14CO over-layer corresponding to $\theta = 0.875$. (c) 1×10^5 Pa CO. In (b) and (c), red and yellow rectangles show locations of quasi-top CO molecules and quasi-bridge CO molecules, respectively. White arrows indicate direction of scan profiles which are shown on the right side. Settings for STM acquisition are: (a) 0.50 nA, 0.60 V; (b) 1.00 nA, 0.60 V; (c) 0.85 nA, 0.90 V.

With increasing chemical potential, coverage increases and CO molecules arrange in a similar manner on a longer unit cell - (6×2) -10CO, corresponding to a coverage of 0.83 ML. At this coverage, in a similar way to the (4×2) unit cell case, we find that two configurations of CO molecules on the surface have similar adsorption energies - (i) 6 CO on top (and quasi-top) + 4 CO on quasi-bridge CO (ii) 4 CO on quasi-top + 6 CO bridge and quasi-bridge

(structures X and XI in table 5. The former orientation is only stable at high temperatures ($T > 370$ K) and high pressures ($P > 6 \times 10^4$ Pa). At the quasi-top/quasi-bridge site the adsorbed CO are tilted from the normal z-axis by a $\pm 5.5^\circ$ angle. Such a behaviour of “fan out” helps to incorporate more adsorbate on the surface and similar observation was made previously on 2D nano-clusters on reconstructed hex-Pt(100) surface in CO environments by Tao. et. al.⁷⁵.

Finally we see that the coverage saturates at 0.875 ML where two iso-energy CO configurations, (i) 8 quasi-top, 6 quasi-bridge and (ii) 6 quasi-top, 8 quasi-bridge CO adsorbed on a (8×2) unit cell are stable (structures XII and XII-a in Table 5). The quasi-top adsorbed CO are tilted at an angle of $\pm 6^\circ$ and the quasi-bridge adsorbed CO are tilted at an angle of $\pm 5.2^\circ$ with respect to the normal z-axis.

Beyond the already discussed low pressure conditions, a high CO pressure was studied experimentally to confirm the predictions from theory (Fig. 4(b) and (c)). Two experiments were performed at rather similar near ambient pressure (6.6×10^4 Pa and 10^5 Pa). At 6.6×10^4 Pa, they formed a (8×2) -14CO over-layer structure, in agreement with the computed stability diagram (blue dots in Fig. 3). Two groups of bright protrusion in the STM can be identified (red rectangles = 3 higher protrusions, yellow rectangles = 4 lower protrusion) in Fig. 4(b) and 4(c), indicating the presence of quasi-top and quasi-bridge CO. DFT Simulated STM image of this structure (SI Fig. S11) shows brighter contrast of CO on top/quasi-top site compared to CO on bridge/quasi-bridge sites. Therefore, based on the contrast of the experimental STM image (fig. 4(b) and 4(c)), it can be deduced that configuration (i) (6 quasi-top, 8 quasi-bridge), of the two iso-energetic CO configurations mentioned earlier, is the one being observed experimentally. Interestingly, configuration (ii) (8 quasi-top, 6 quasi-bridge) was not observed in STM images.

On further examination of high coverage ($\theta \geq 0.75$) structures for Pt(100), CO arranges in a skewed hexagonal matrix with average CO-CO distances smaller than that observed on Pt(111). On Pt(111), at $\theta = 0.75$, CO arranges on a $p(2 \times 2)$ unit cell with CO on top, FCC and

HCP site creating a perfect hexagonal lattice with C-C distance of 3.25 Å. In comparison, for Pt(100), the average C-C distance for CO on (4x2), (6x2) and (8x2) is 3.22 (2.22% smaller), 3.18 (3.4%) and 2.93 (11.02%) respectively. The superimposed distorted hexagonal configuration of CO on Pt(100) reduces the repulsion between adjacent CO molecules and therefore decreases the energy. Hence for a given condition (for example standard condition at room temperature) the density of chemisorbed CO molecules is larger on Pt(100) (0.11 in CO/Å²) than on Pt(111) (0.099 in CO/Å²). This is due to the lower Pt-Pt coordination on Pt(100) resulting in a larger CO adsorption energy, that is able to compensate a stronger CO-CO repulsion energy and lead to a larger CO density at equilibrium. It's worth highlighting that using the generalized correction, $\Delta = 4.77d_{CO} - 5.37$ eV, results in essentially the same stability diagram (SI Fig. S11) as using the separately fitted correction terms for Pt(100) surface ($\Delta = 4.74d_{CO} - 5.34$ eV).

4 Conclusion

The adsorption of CO on Pt(111) and Pt(100) was studied using an atomistic first-principles thermodynamic model and high pressure scanning tunneling microscopy. In order to correct for the site preference and for the overestimated adsorption energy, we developed a energy correction scheme based on the C-O bond distance. The magnitude of the correction is smallest for the top site, followed by the bridge and other poly-coordinated sites (threefold hcp/fcc site for Pt(111) and fourfold hollow site for Pt(100)). Using the energy correction scheme, we construct the thermodynamic stability diagram that describes the surface terminations as a function of temperature and pressure. The formation of dense CO layers on Pt(111) and Pt(100) follow two different modes. On Pt(111) (at $\theta=0.25$ ML) all the adsorption sites (top, bridge, hollow) are rather equivalent in stability. In order to optimize adsorption and minimize repulsion CO molecules organize in a 2D hexagonal pattern and the adsorbate density depends on the pressure. This CO hexagonal pattern is set in registry

with the surface by the coincidence of a rotated supercell of Pt(111) with a rotated supercell of the CO hexagonal lattice. From this ideal starting position, CO molecules slightly relax laterally, with also small tilts with respect to the vertical direction, and slightly deform the hexagonal pattern. A systematic computational exploration of such hexagonal coincidence structures shows that the $(2\sqrt{3} \times 2\sqrt{3})R30^\circ$ -7CO at 0.583 ML and the $(\sqrt{19} \times \sqrt{19})R23.4^\circ$ -13CO at 0.684 ML are the stable arrangement appearing in the calculated thermodynamic diagram. These calculated structures are in very good agreement with experimental data, as seen for example with the simulated STM image (refer figure S5 in Supporting Information). Non-hexagonal CO adlayers ($(\sqrt{3} \times 3)$ rect-4CO and $c(\sqrt{3} \times 7)$ rect-5CO arrangement) however appear as low energy metastable structures, explaining why in UHV at low temperature, these non-hexagonal layers can be observed in place of the Moiré pattern coincidence lattices.

On Pt(100), bridge and top sites have similar stability, but the hollow site is less stable. The CO molecules hence adopt a 1D coincidence lattice, with $n-1$ CO molecules placed on a dense row of n Pt atoms, with an ensemble of top sites molecules followed by an ensemble of bridge site ones. The structures relax with slight off vertical rotations on the CO molecules, illustrated as a “fan-out” movement. These “fan-out” displacements lead to reduced repulsion between CO molecules on adjacent adsorption sites. These CO rows are staggered in the perpendicular direction, forming elongated $(n \times 2)$ unit cells. Our STM experiments at ambient CO pressure and room temperature on Pt(100) clearly confirm these theoretical predictions, with the formation of a highly dense (8×2) -14CO structure (coverage of 0.875 ML). These high coverage structures of CO provide structural data for the study of the catalytic reactivity and restructuring events occurring on these Pt surfaces in reactions involving high CO pressures.

4.1 Acknowledgment

This work was funded by NSF, Grant No. 1800601. This work used computational and storage services associated with the Hoffman2 Shared Cluster provided by the UCLA Institute for Digital Research and Education's Research Technology Group. The authors want to thank XSEDE (TG-CHE170060) SDSC's Comet Supercomputer and Bridges PSC for the compute time.

References

- (1) Chorkendorff, I.; Niemantsverdriet, J. W. *Concepts of modern catalysis and kinetics*; Wiley Online Library, 2003; Vol. 138.
- (2) Allian, A. D.; Takanabe, K.; Furdala, K. L.; Hao, X.; Truex, T. J.; Cai, J.; Buda, C.; Neurock, M.; Iglesia, E. Chemisorption of CO and mechanism of CO oxidation on supported platinum nanoclusters. *Journal of the American Chemical Society* **2011**, *133*, 4498–4517.
- (3) Chua, Y. G.; Gunasooriya, G. K. K.; Saeys, M.; Seebauer, E. G. Controlling the CO oxidation rate over Pt/TiO₂ catalysts by defect engineering of the TiO₂ support. *Journal of catalysis* **2014**, *311*, 306–313.
- (4) Eichler, A. CO oxidation on transition metal surfaces: reaction rates from first principles. *Surface science* **2002**, *498*, 314–320.
- (5) Fu, Q.; Saltsburg, H.; Flytzani-Stephanopoulos, M. Active nonmetallic Au and Pt species on ceria-based water-gas shift catalysts. *Science* **2003**, *301*, 935–938.
- (6) Rodriguez, J.; Ma, S.; Liu, P.; Hrbek, J.; Evans, J.; Perez, M. Activity of CeO_x and TiO_x nanoparticles grown on Au (111) in the water-gas shift reaction. *Science* **2007**, *318*, 1757–1760.

- (7) Lin, C.-H.; Chen, C.-L.; Wang, J.-H. Mechanistic studies of water–gas-shift reaction on transition metals. *The Journal of Physical Chemistry C* **2011**, *115*, 18582–18588.
- (8) Grabow, L. C.; Gokhale, A. A.; Evans, S. T.; Dumesic, J. A.; Mavrikakis, M. Mechanism of the water gas shift reaction on Pt: First principles, experiments, and microkinetic modeling. *The Journal of Physical Chemistry C* **2008**, *112*, 4608–4617.
- (9) Dry, M. E. The fischer–tropsch process: 1950–2000. *Catalysis today* **2002**, *71*, 227–241.
- (10) Khodakov, A. Y.; Chu, W.; Fongarland, P. Advances in the development of novel cobalt Fischer- Tropsch catalysts for synthesis of long-chain hydrocarbons and clean fuels. *Chemical reviews* **2007**, *107*, 1692–1744.
- (11) Den Breejen, J.; Radstake, P.; Bezemer, G.; Bitter, J.; Frøseth, V.; Holmen, A.; De Jong, K. On the origin of the cobalt particle size effects in Fischer- Tropsch catalysis. *Journal of the American Chemical Society* **2009**, *131*, 7197–7203.
- (12) Somorjai, G. A.; Li, Y. *Introduction to surface chemistry and catalysis*; John Wiley & Sons, 2010.
- (13) Avery, N. R. Electron energy loss spectroscopic study of CO on Pt (111). *The Journal of chemical physics* **1981**, *74*, 4202–4203.
- (14) Shigeishi, R.; King, D. A. Chemisorption of carbon monoxide on platinum {111}: Reflection-absorption infrared spectroscopy. *Surface Science* **1976**, *58*, 379–396.
- (15) Crossley, A.; King, D. A. Infrared spectra for co isotopes chemisorbed on Pt “111”: Evidence for strong adsorbate coupling interactions. *Surface Science* **1977**, *68*, 528–538.
- (16) Ertl, G.; Neumann, M.; Streit, K. Chemisorption of CO on the Pt (111) surface. *Surface Science* **1977**, *64*, 393–410.

- (17) Hopster, H.; Ibach, H. Adsorption of CO on Pt (111) and Pt 6 (111)×(111) studied by high resolution electron energy loss spectroscopy and thermal desorption spectroscopy. *Surface Science* **1978**, *77*, 109–117.
- (18) Steininger, H.; Lehwald, S.; Ibach, H. On the adsorption of CO on Pt (111). *Surface Science* **1982**, *123*, 264–282.
- (19) Hayden, B.; Bradshaw, A. *Studies in Surface Science and Catalysis*; Elsevier, 1983; Vol. 14; p 51.
- (20) Bibberian, J.; Van Hove, M. A new model for CO ordering at high coverages on low index metal surfaces: A correlation between LEED, HREELS and IRS: II. CO adsorbed on fcc (111) and hep (0001) surfaces. *Surface science* **1984**, *138*, 361–389.
- (21) Tüshaus, M.; Schweizer, E.; Hollins, P.; Bradshaw, A. Yet another vibrational study of the adsorption system Pt {111}-CO. *Journal of electron spectroscopy and related phenomena* **1987**, *44*, 305–316.
- (22) Kiskinova, M.; Szab, A.; Yates Jr, J. Compressed CO overlayers on Pt (111)—evidence for tilted CO species at high coverages by digital ESDIAD. *Surface Science* **1988**, *205*, 215–229.
- (23) Schweizer, E.; Persson, B.; Tüshaus, M.; Hoge, D.; Bradshaw, A. The potential energy surface, vibrational phase relaxation and the order-disorder transition in the adsorption system Pt {111}-CO. *Surface Science* **1989**, *213*, 49–89.
- (24) Brown, W.; Kose, R.; King, D. Femtomole adsorption calorimetry on single-crystal surfaces. *Chemical reviews* **1998**, *98*, 797–832.
- (25) Lee, W.; Ford, L.; Blowers, P.; Nigg, H.; Masel, R. Why do heats of adsorption of simple gases on platinum surfaces vary so little with surface structure? *Surface science* **1998**, *416*, 141–151.

- (26) Yang, H. J.; Minato, T.; Kawai, M.; Kim, Y. STM Investigation of CO ordering on Pt (111): From an isolated molecule to high-coverage superstructures. *The Journal of Physical Chemistry C* **2013**, *117*, 16429–16437.
- (27) McCrea, K.; Parker, J. S.; Chen, P.; Somorjai, G. Surface structure sensitivity of high-pressure CO dissociation on Pt (557), Pt (100) and Pt (111) using sum frequency generation surface vibrational spectroscopy. *Surface science* **2001**, *494*, 238–250.
- (28) Norton, P.; Davies, J.; Jackman, T. Absolute coverages of CO and O on Pt (111); comparison of saturation CO coverages on Pt (100),(110) and (111) surfaces. *Surface Science Letters* **1982**, *122*, L593–L600.
- (29) Yeo, Y.; Vattuone, L.; King, D. Energetics and kinetics of CO and NO adsorption on Pt {100}: Restructuring and lateral interactions. *The Journal of chemical physics* **1996**, *104*, 3810–3821.
- (30) Behm, R.; Thiel, P.; Norton, P.; Ertl, G. The interaction of CO and Pt (100). I. Mechanism of adsorption and Pt phase transition. *The Journal of Chemical Physics* **1983**, *78*, 7437–7447.
- (31) Song, M.-B.; Yoshimi, K.; Ito, M. STM observations of bridge-bonded CO on Pt (111) and asymmetric on-top CO on Pt (100). *Chemical physics letters* **1996**, *263*, 585–590.
- (32) Martin, R.; Gardner, P.; Bradshaw, A. The adsorbate-induced removal of the Pt {100} surface reconstruction. Part II: CO. *Surface science* **1995**, *342*, 69–84.
- (33) Maniguet, S.; Mathew, R. J.; Russell, A. E. EXAFS of carbon monoxide oxidation on supported Pt fuel cell electrocatalysts. *The Journal of Physical Chemistry B* **2000**, *104*, 1998–2004.
- (34) Guo, N.; Fingland, B. R.; Williams, W. D.; Kispersky, V. F.; Jelic, J.; Delgass, W. N.; Ribeiro, F. H.; Meyer, R. J.; Miller, J. T. Determination of CO, H₂O and H₂ coverage by

- XANES and EXAFS on Pt and Au during water gas shift reaction. *Physical Chemistry Chemical Physics* **2010**, *12*, 5678–5693.
- (35) Lahee, A.; Toennies, J.; Wöll, C. Low energy adsorbate vibrational modes observed with inelastic helium atom scattering: CO on Pt (111). *Surface Science* **1986**, *177*, 371–388.
- (36) Björneholm, O.; Nilsson, A.; Tillborg, H.; Bennich, P.; Sandell, A.; Herdnäs, B.; Puglia, C.; Mårtensson, N. Overlayer structure from adsorbate and substrate core level binding energy shifts: CO, CCH₃ and O on Pt (111). *Surface science* **1994**, *315*, L983–L989.
- (37) Persson, B.; Tüshaus, M.; Bradshaw, A. On the nature of dense CO adlayers. *The Journal of chemical physics* **1990**, *92*, 5034–5046.
- (38) Longwitz, S. R.; Schnadt, J.; Vestergaard, E. K.; Vang, R. T.; Lægsgaard, E.; Stensgaard, I.; Brune, H.; Besenbacher, F. High-coverage structures of carbon monoxide adsorbed on Pt (111) studied by high-pressure scanning tunneling microscopy. *The Journal of Physical Chemistry B* **2004**, *108*, 14497–14502.
- (39) Gunasooriya, G. K. K.; Saeys, M. CO Adsorption on Pt (111): From Isolated Molecules to Ordered High-Coverage Structures. *ACS Catalysis* **2018**, *8*, 10225–10233.
- (40) Bocquet, M.-L.; Sautet, P. STM and chemistry: a qualitative molecular orbital understanding of the image of CO on a Pt surface. *Surface science* **1996**, *360*, 128–136.
- (41) Kresse, G.; Gil, A.; Sautet, P. Significance of single-electron energies for the description of CO on Pt (111). *Physical Review B* **2003**, *68*, 073401.
- (42) Abild-Pedersen, F.; Andersson, M. CO adsorption energies on metals with correction for high coordination adsorption sites—A density functional study. *Surface Science* **2007**, *601*, 1747–1753.

- (43) Gajdoš, M.; Eichler, A.; Hafner, J. CO adsorption on close-packed transition and noble metal surfaces: trends from ab initio calculations. *Journal of Physics: Condensed Matter* **2004**, *16*, 1141.
- (44) Feibelman, P. J.; Hammer, B.; Nørskov, J. K.; Wagner, F.; Scheffler, M.; Stumpf, R.; Watwe, R.; Dumesic, J. The CO/Pt (111) puzzle. *The Journal of Physical Chemistry B* **2001**, *105*, 4018–4025.
- (45) Hu, Q.-M.; Reuter, K.; Scheffler, M. Towards an exact treatment of exchange and correlation in materials: Application to the “CO adsorption puzzle” and other systems. *Physical review letters* **2007**, *98*, 176103.
- (46) Schimka, L.; Harl, J.; Stroppa, A.; Grüneis, A.; Marsman, M.; Mittendorfer, F.; Kresse, G. Accurate surface and adsorption energies from many-body perturbation theory. *Nature materials* **2010**, *9*, 741.
- (47) Gautier, S.; Steinmann, S. N.; Michel, C.; Fleurat-Lessard, P.; Sautet, P. Molecular adsorption at Pt (111). How accurate are DFT functionals? *Physical Chemistry Chemical Physics* **2015**, *17*, 28921–28930.
- (48) Duanmu, K.; Truhlar, D. G. Validation of density functionals for adsorption energies on transition metal surfaces. *Journal of chemical theory and computation* **2017**, *13*, 835–842.
- (49) Wellendorff, J.; Silbaugh, T. L.; Garcia-Pintos, D.; Nørskov, J. K.; Bligaard, T.; Studt, F.; Campbell, C. T. A benchmark database for adsorption bond energies to transition metal surfaces and comparison to selected DFT functionals. *Surface Science* **2015**, *640*, 36–44.
- (50) Wang, Y.; de Gironcoli, S.; Hush, N. S.; Reimers, J. R. Successful a priori modeling of CO adsorption on pt (111) using periodic hybrid density functional theory. *Journal of the American Chemical Society* **2007**, *129*, 10402–10407.

- (51) Doll, K. CO adsorption on the Pt (1 1 1) surface: a comparison of a gradient corrected functional and a hybrid functional. *Surface science* **2004**, *573*, 464–473.
- (52) Blyholder, G. Molecular orbital view of chemisorbed carbon monoxide. *The Journal of Physical Chemistry* **1964**, *68*, 2772–2777.
- (53) Hammer, B.; Morikawa, Y.; Nørskov, J. K. CO chemisorption at metal surfaces and overlayers. *Physical review letters* **1996**, *76*, 2141.
- (54) Gil, A.; Clotet, A.; Ricart, J. M.; Kresse, G.; Garcia-Hernández, M.; Rösch, N.; Sautet, P. Site preference of CO chemisorbed on Pt (1 1 1) from density functional calculations. *Surface science* **2003**, *530*, 71–87.
- (55) Mason, S. E.; Grinberg, I.; Rappe, A. M. First-principles extrapolation method for accurate CO adsorption energies on metal surfaces. *Physical Review B* **2004**, *69*, 161401.
- (56) Van Santen, R. A.; Neurock, M. *Molecular heterogeneous catalysis: a conceptual and computational approach*; John Wiley & Sons, 2009.
- (57) Held, G.; Schuler, J.; Sklarek, W.; Steinrück, H.-P. Determination of adsorption sites of pure and coadsorbed CO on Ni (111) by high resolution X-ray photoelectron spectroscopy. *Surface science* **1998**, *398*, 154–171.
- (58) Talbi, D.; Chandler, G. Extensive ab Initio Study of the C₂O₂, C₂S₂, and C₂OS Systems: Stabilities and Singlet- Triplet Energy Gaps. *The Journal of Physical Chemistry A* **2000**, *104*, 5872–5881.
- (59) Tao, F.; Nguyen, L.; Zhang, S. Design of a new reactor-like high temperature near ambient pressure scanning tunneling microscope for catalysis studies. *Review of Scientific Instruments* **2013**, *84*, 034101.
- (60) Koper, M. T.; van Santen, R. A.; Wasileski, S. A.; Weaver, M. J. Field-dependent chemisorption of carbon monoxide and nitric oxide on platinum-group (111) surfaces:

- Quantum chemical calculations compared with infrared spectroscopy at electrochemical and vacuum-based interfaces. *The Journal of Chemical Physics* **2000**, *113*, 4392–4407.
- (61) Illas, F.; Zurita, S.; Rubio, J.; Marquez, A. Origin of the vibrational shift of CO chemisorbed on Pt (111). *Physical Review B* **1995**, *52*, 12372.
- (62) Yeo, Y.; Vattuone, L.; King, D. Calorimetric heats for CO and oxygen adsorption and for the catalytic CO oxidation reaction on Pt {111}. *The Journal of chemical physics* **1997**, *106*, 392–401.
- (63) Tao, F.; Crozier, P. A. Atomic-scale observations of catalyst structures under reaction conditions and during catalysis. *Chemical reviews* **2016**, *116*, 3487–3539.
- (64) Teschner, D.; Révay, Z.; Borsodi, J.; Hävecker, M.; Knop-Gericke, A.; Schlögl, R.; Milroy, D.; Jackson, S. D.; Torres, D.; Sautet, P. Understanding palladium hydrogenation catalysts: when the nature of the reactive molecule controls the nature of the catalyst active phase. *Angewandte Chemie International Edition* **2008**, *47*, 9274–9278.
- (65) Reuter, K.; Scheffler, M. Composition and structure of the RuO₂ (110) surface in an O₂ and CO environment: Implications for the catalytic formation of CO₂. *Physical Review B* **2003**, *68*, 045407.
- (66) Michaelides, A.; Bocquet, M.-L.; Sautet, P.; Alavi, A.; King, D. Structures and thermodynamic phase transitions for oxygen and silver oxide phases on Ag {1 1 1}. *Chemical physics letters* **2003**, *367*, 344–350.
- (67) van Spronsen, M. A.; Daunmu, K.; O'Connor, C. R.; Egle, T.; Kersell, H.; Oliver-Meseguer, J.; Salmeron, M. B.; Madix, R. J.; Sautet, P.; Friend, C. M. Dynamics of Surface Alloys: Rearrangement of Pd/Ag (111) Induced by CO and O₂. *The Journal of Physical Chemistry C* **2018**, *123*, 8312–8323.

- (68) Ogletree, D.; Van Hove, M.; Somorjai, G. LEED intensity analysis of the structures of clean Pt (111) and of CO adsorbed on Pt (111) in the c (4× 2) arrangement. *Surface science* **1986**, *173*, 351–365.
- (69) Blackman, G.; Xu, M.-L.; Ogletree, D.; Van Hove, M.; Somorjai, G. Mix of molecular adsorption sites detected for disordered CO on Pt (111) by diffuse low-energy electron diffraction. *Physical review letters* **1988**, *61*, 2352.
- (70) Pedersen, M. Ø.; Bocquet, M.-L.; Sautet, P.; Lægsgaard, E.; Stensgaard, I.; Besenbacher, F. CO on Pt (111): binding site assignment from the interplay between measured and calculated STM images. *Chemical physics letters* **1999**, *299*, 403–409.
- (71) Petrova, N.; Yakovkin, I. Lateral interaction and CO adlayer structures on the Pt (111) surface. *Surface science* **2002**, *519*, 90–100.
- (72) Villegas, I.; Weaver, M. J. Carbon monoxide adlayer structures on platinum (111) electrodes: A synergy between in-situ scanning tunneling microscopy and infrared spectroscopy. *The Journal of chemical physics* **1994**, *101*, 1648–1660.
- (73) Loffreda, D.; Simon, D.; Sautet, P. Dependence of stretching frequency on surface coverage and adsorbate–adsorbate interactions: a density-functional theory approach of CO on Pd (111). *Surface science* **1999**, *425*, 68–80.
- (74) Brodén, G.; Pirug, G.; Bonzel, H. Chemisorption of CO on the unreconstructed Pt (100) surface. *Surface Science* **1978**, *72*, 45–52.
- (75) Tao, F.; Dag, S.; Wang, L.-W.; Liu, Z.; Butcher, D. R.; Salmeron, M.; Somorjai, G. A. Restructuring of hex-Pt (100) under CO gas environments: formation of 2-D nanoclusters. *Nano letters* **2009**, *9*, 2167–2171.

Graphical TOC Entry

